ROYAL SOCIETY OF CHEMISTRY

Journal Name

ARTICLE

Direct and Converse Piezoelectric Responses at the Nanoscale from Epitaxial BiFeO₃ Thin Films Grown by Polymer Assisted Deposition

José Manuel Vila-Fungueiriño*[a], Andrés Gómez*[b], J. Antoja-Lleonart[e], Jaume Gázquez[b], César Magén[c,d], B. Noheda[e] and Adrián Carretero-Genevrier*[a]

We use an original water-based chemical method, to grow pure epitaxial BiFeO₃ (BFO) ultra-thin films with excellent piezoelectric properties. Particularly, we show that this novel chemical route produces a higher natural ferroelectric domain size distribution and coercive field compared to similar BFO films grown by physical methods. Moreover, we measured the d_{33} piezoelectric coefficient of 60 nm thick BFO films with a direct approach, using Direct Piezoelectric Force Microscopy (DPFM). As a result, first piezo-generated charge maps of a very thin BFO layer were obtained applying this novel technology. We also performed a comparative study of the d_{33} coefficients between standard PFM analysis and the DPFM microscopy showing similar values i.e. 17 pm/V and 22 pC/N respectively. Finally, we proved that the directionality of the piezoelectric effect in BFO ferroelectric thin films is preserved at low thickness dimensions demonstrating the potential of chemical processes for the development of low cost functional ferroelectric and piezoelectric devices.

1. Introduction

Ferroelectric oxides are materials that combine properties of memory, piezoelectricity, and pyroelectricity providing solutions to many technological challenges including lower energy consumption devices and inertial sensors for distance, movement and acceleration detection.[1] Rhombohedral bismuth ferrite (BiFeO₃, BFO) is a paradigmatic example of ferroelectric perovskite oxide with giant remanent polarization P_r ca. 100 μCcm⁻² at room temperature along $[111]_{pseudocubic}$ direction and robust antiferromagnetic and ferroelastic orders. In particular, BFO has three types of ferroelectric domain walls according to their polarization vectors: 71°, 109°, and 180° walls. [2-5] BFO thin films have been extensively studied due to a large polarization, in spite of a relatively low piezoelectric coefficient ($d_{33} \approx$ 15-60 pmV⁻¹) compared to PbZr$_x$Ti$_{1-x}$O₃, PZT.[6-]

[8] However, the large leakage current observed in this material represents an important obstacle for the practical usage of BFO-based devices.[9] Especially, the electrical conductive nature of BFO hinders the achievement of excellent ferroelectric properties at the macroscale. For that reason, the possibility of controlling at the nanoscale the formation of ferroelectric domains in epitaxial (001) BFO thin films makes this material keen for applications such as data storage or optical frequency converters.[10, 11] However, as BFO is not a natural mineral, secondary phases can be easily formed during its synthesis.[12] For this reason, the preparation of high quality epitaxial BFO thin films requires a perfect control of the oxygen pressure, temperature, stoichiometry and crystallization. In spite of these difficulties, Wang et al.[6] and other groups have obtained high-quality epitaxial BFO thin films employing physical methods such as PLD[13-16], sputtering[17-19] or MBE[20, 21] to obtain high-quality epitaxial BFO thin films with enhanced polarization.[15] High-vacuum methods offer unique advantages including high crystal quality and precise control of composition and thickness at atomic scale.[22] Unfortunately, these methodologies are not compatible with inexpensive large-scale manufacturing processes. Conversely, Chemical Solution Deposition (CSD) methods are adapted for large area coating by an easy and low cost implementation.[23] Recently, several works have reported functional CSD-derived BFO thin films,[24-28] although their quality were usually lower than those prepared by high-vacuum methods,[29] including secondary phases in most of the cases.

a. Institut d'Électronique et des Systèmes (IES), UMR 5214, CNRS – Université de Montpellier, 860 rue Saint Priest, 34095 Montpellier, France. e-mail: adrien.carretero@ies.univ-montp2.fr, jose-manuel.vila@ies.univ-montp2.fr
b. Institut de Ciència de Materials de Barcelona ICMAB, Consejo Superior de Investigacions Científiques CSIC, Campus UAB 08193 Bellaterra, Catalonia, Spain. e-mail: agomez@icmab.es
c. Instituto de Ciencia de Materiales de Aragón (ICMA), Universidad de Zaragoza-CSIC, Facultad de Ciencias, Universidad de Zaragoza, Pedro Cerbuna 12, 50009 Zaragoza, Spain.
d. Laboratorio de Microscopías Avanzadas (LMA), Instituto de Nanociencia de Aragón (INA), Universidad de Zaragoza, Mariano Esquillor, Edificio I+D, 50018 Zaragoza, Spain.
e. Zernike Institute for Advanced Materials, University of Groningen, Nijenborgh 4, 9747 AG Groningen, The Netherlands.

ARTICLE   **Journal Name**

Among CSD techniques, Polymer Assisted Deposition (PAD), a soft-chemistry technique introduced by Jia *et al.*[30], has proved to be one of the most suitable processes to produce high quality epitaxial complex and multilayer-structured films in the very thin range below 100 nm.[31-33] PAD uses branched polymers to coordinate, stabilize cations in an aqueous solution from soluble metal sources (nitrates or chlorides), and provide the adequate viscosity to the solution which finally is homogeneously spin-coated on a substrate.[34] Contrarily to other CSD methods that employ alkoxides as metal sources and/or organic solvents such as 2-methoxyethanol or ethylene glycol, PAD uses a free-environment water based fabrication with very easy chemical tasks. The compositional stability provided by PAD is crucial for the synthesis of BFO due to multiple synthetic difficulties (phase impurities, iron oxide segregation, bismuth volatilization, etc.)[35, 36].

In this paper, we report the growth of full (001)-oriented piezoelectric and ferroelectric BFO thin films (≈30-60 nm) with high crystalline quality on $SrTiO_3$ (STO) substrates by PAD. X-Ray Diffraction (XRD) and Scanning Transmission Electron Microscopy (STEM) cross section analysis confirmed a complete epitaxial crystallization at 650°C. Direct and indirect nanoscale measurements of piezoelectric coefficient d_{33} and ferroelectric domains were obtained by Piezoresponse Force Microscopy (PFM) and Direct Piezoelectric Force Microscopy (DPFM).[37] PFM analysis were used to image disclose the in-plane and out-of-plane configuration of epitaxial BFO thin films. PFM spectroscopy analysis allowed the measuring of local ferroelectric hysteresis loops and the generation and recording of on-demand domain structures. Remarkably, we report the first images of the piezo-generated charge of BFO 60 nm-thick thin films grown by a chemical method. DPFM permits to disclose the complex domain structure generation and, more importantly, the specific d_{33} value obtained with this methodology. We compare the d_{33} acquired from a direct approach with that obtained by the piezoelectric converse approach, in which it is possible to deduce that the bidirectionality of the piezoelectric effect is preserved at this nanoscale regime.

2. Results and discussion

X-ray diffraction analysis shown in **Figure 1** indicates the oriented growth, high crystallinity and epitaxial matching of 30 nm-thick BFO films on STO single crystal substrate. Synchrotron long scan diffraction patterns from 1 to 4 Miller index (**Figure 1a**) shows the absence of secondary phases and the existence of only (00*l*) Bragg peaks from BFO. The rocking curve around the (002) peak of BFO evidences the high crystallinity achieved at 650°C with a FWHM 0.12° value similar to a bulk single crystal. At higher temperatures, i.e. 900°C, BFO crystal structure is not stable and disappears and only the iron signal coming from (012)-oriented α-Fe_2O_3 (hematite) is detected by Energy-Dispersive X-ray (EDX) elemental analysis (**Figure S1**). Therefore, only BFO samples grown at the temperature range of 600-650°C have a good crystalline and surface quality, and avoid formation of iron oxide impurities
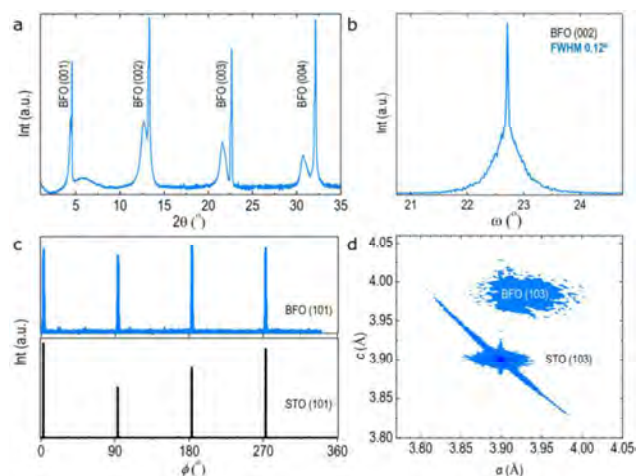

Figure 1. a) Synchrotron XRD pattern of the BFO film in a θ-2θ configuration. b) Rocking curve recorded around the (002) reflection of BFO showing a FWHM value of 0.12°. c) Phi-scan of the (101) peak of the (001)-oriented BFO film. d) Real space representation from a Reciprocal Space Mapping (RSM) around the (103) Bragg peak of the perovskite containing both the STO substrate and the BFO film.

that start to crystallize at 700°C (**Figure S2**, **S3 S4, S5**).[35] The out-of-plane lattice parameter $c_{BFO}^{pc} = 4.012$ Å is larger than the bulk counterpart due to the compressive strain imposed by the STO substrate and resulting in a tetragonal-like crystal structure. This feature is in agreement with other films previously reported with thickness values below 100 nm.[6] Phi scan and Reciprocal Space Mapping

(RSM) taken in Bragg reflections containing both in-plane and out-of-plane lattice parameters illustrate the cube-on-cube growth of BFO thin films. These crystallographic results confirm that the epitaxial strain of BFO films is effectively and similarly transferred using PAD process or high-vacuum process.

Epitaxial growth and interface quality of BFO films were further investigated by High Angle Annular Dark Field (HAADF) imaging in high-resolution STEM mode. This imaging mode provides images the intensity of which scales with the square of the atomic number, referred to as Z-contrast images. **Figure 2** and S6 show cross-sectional view of a BFO film grown at 650°C on STO substrate with no structural and chemical defects. Moreover, atomic resolution Z-contrast image of the interface reveals the coherent epitaxial growth of BFO layer
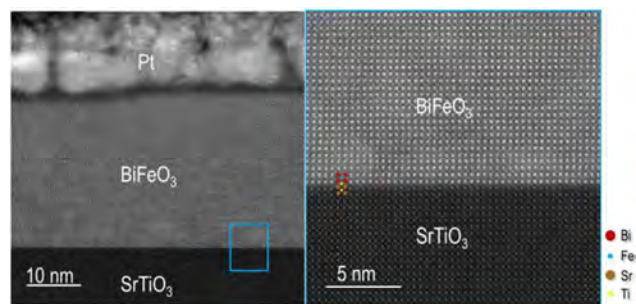

Figure 2. Atomic resolution HAADF-STEM image of the pseudocubic (001)-oriented BFO thin film viewed along the [100]-crystallographic direction. Detail of the HAADF image showing the coherent interface between the BFO and the STO substrate (right image).
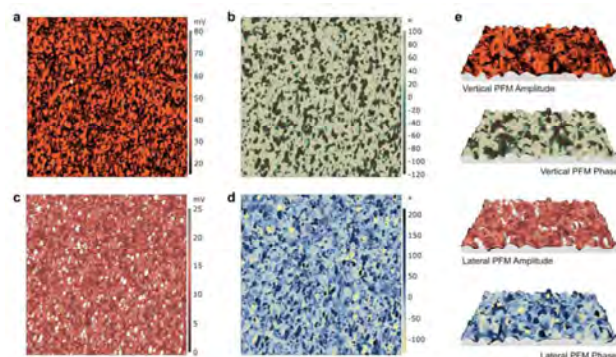
Nanoscale

Journal Name

ARTICLE

Figure 3. Piezoresponse Force Microscopy imaging (5 × 5 μm) of natural domains of the (001)-oriented 30 nm thick BFO film. **a** and **b** Vertical PFM Amplitude and Phase, respectively; **c** and **d** Lateral PFM Amplitude and Phase, respectively and **e** 3D representation of the PFM color images overlapped into Topographic information roughness. Images are collected simultaneously, 4 VAC bias applied at a frequency of 20 kHz, with applied force of 300 nN and scan rate 0.5 ln/s.

with an atomically sharp interface with the STO substrate.

Natural ferroelectric domain structure of epitaxial 30 nm thick BFO film on STO substrate was investigated using Piezoresponse Force Microscopy (PFM)[38] at room temperature (**Figure 3**). BFO possesses complex domain configurations, from which the natural polarization can be settled to different angles: 0°; 71°; 109° and 180°.[8] In order to decipher the specific domain structure, both the vertical PFM Amplitude and Phase, **Figure 3a** and **3b**, and the Lateral PFM Amplitude and Phase, **Figure 3c** and **3d**, were recorded, respectively. From these images, the average domain size of 30 nm thick BFO films was calculated, providing a value of 0.094 μm^2 obtained from **Figure 3a**, which is two times higher than other BFO films with 40 nm thick grown on STO substrates by physical methods.[39] Thus, our results show that the PAD process can modify the ferroelectric domain size, as this methodology employs low temperatures synthesis that may induces a growth regime closer to the thermodynamic equilibrium, as compared to physical methods[34], which may change the settling of the natural domain structure. More importantly, the specific domain distribution of BFO films was studied by calculating the specifics histograms related to the Lateral and Vertical PFM phase images, see **Figure S7**. By using the method outlined by Kalinin *et al.*[40], it is possible to obtain the polarization orientation from the Vertical and Lateral PFM images. From this methodology, VPFM gives the out-of-plane component of the polarization, while LPFM provides the in-plane component, see **Figure S7**. From all the possible polarization vector of BFO we conclude that the 109° natural domain orientation is predominant in our BFO thin films, which corresponds to the energetically favorable orientation as previously determined by Lubk *et al.*[41, 42]

The ferroelectric switching of 60 nm and 30 nm thick epitaxial BFO films was also investigated, by growing a bottom conductive epitaxial La$_{0.7}$Sr$_{0.3}$MnO$_3$ (LSMO) electrode, see **Figure S8 and S9**. Ferroelectricity was assessed on 30 nm thick BFO film (**Figure S10**) and on 60 nm thick BFO film by recording a 3 × 3 μm squared area with a positive sample bias of +7 VDC.
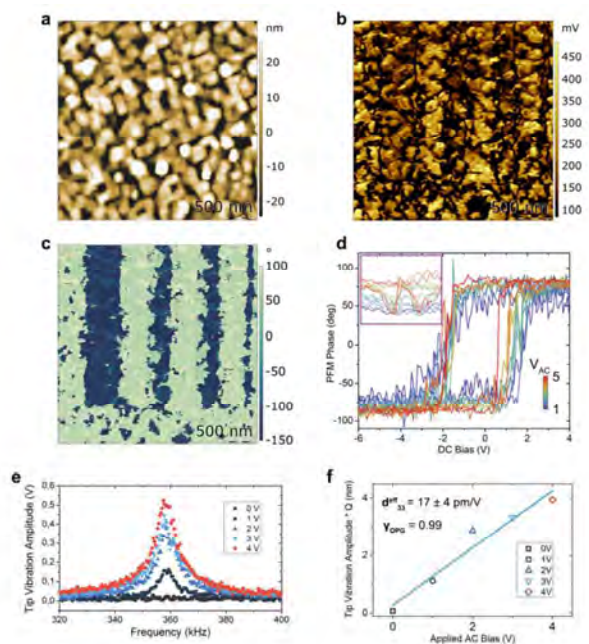

Figure 4. Ferroelectric switching measurements acquired with PFM technique in 60 nm thick epitaxial BFO films grown over a bottom conductive La$_{0.7}$Sr$_{0.3}$MnO$_3$ (LSMO) electrode. **a**, **b** and **c**: Topography, PFM Amplitude and PFM Phase, respectively, of pre-poled area, in which a stripe-like pattern was pre-recorded with a bias voltage of +-7 VDC; scale bar 500 nm. **d** PFM Phase vs Applied DC bias showing PFM ferroelectric-like loop, acquired at the exact same spot, and varying the AC voltage applied to the probe. The PFM Amplitude vs DC Bias is shown in the inset. **e**. Tip vibration Amplitude vs Frequency sweeping between 320 and 400 kHz, at different applied AC bias amplitudes. **f** The maximum tip vibration amplitude, extracted from the acquired frequency sweeps, is plotted vs the applied AC bias. A linear fitting is used to estimate the electromechanical behavior of our films.

Then, a stripe-like pattern was written inside the squared area, with 90° of scan angle, by applying an opposite bias of -7 VDC. After the recording step, the AFM tip was biased with 0 VDC while an AC bias of 2 VAC was applied out-side of the contact resonance. The resulting domain structure is depicted in the **Figure 4a, b** and **c**, which correspond to the topography, the VPFM Phase and the VPFM Amplitude signals, respectively. This set of images shows that the applied electric field, ~ 800 KV/cm, is adequate to switch the BFO natural domain structure to an antiparallel configuration, without any dielectric breakdown, which would result in topographic artifacts. Additional PFM Phase spectroscopy sweeps were performed at the same point by biasing the tip with different AC voltages, first the DC bias was swept from 0 to +7 VDC, and then from +7 to −7 VDC. Finally, a DC bias was switched back to +7 VDC, producing ferroelectric-like loops (**Figure 4d**). The sweeping was repeated with several AC bias amplitudes applied to the tip (**Figure S11**), obtaining a reduction of the coercive field with the applied AC bias. This physical behavior is characteristic of a ferroelectric-like response.[43] The experimental coercive field value of epitaxial BFO films was set to 250 kV/cm, which is substantially higher than those values previously reported in the literature.[44] To obtain such coercive field, a low AC Bias Amplitude of 2VAC was employed. In

ARTICLE

addition, BFO films grown by PAD process present a high switching homogeneity, as denoted by the 4 × 4 matrix array of ferroelectric switching spectroscopies performed in a 5 × 5 µm area, see **Figure S12**. Moreover, the electromechanical response of epitaxial BFO films was studied by using a standard platinum coated tip.[45] Frequency-sweeps were performed in order to depict the first contact resonance point, see **Figure 4e**. The sweeps were repeated with different applied AC bias magnitudes, which provided the maximum displacement for each applied voltage amplitude.[46, 47] A linear response with the applied AC bias was obtained allowing the estimation of the electromechanical response of BFO films i.e. the d_{33}^{PFM} value. The obtained value for a BFO film of 60 nm thick is 17±4 pm/V, in agreement with other values previously reported.[45] Notice that the acquisition of an open piezo-potential gauge, γ_{OPG} of nearly 1, ensure the piezoelectric response without a substantial force that could reduce its movement and, consequently, the d_{33} constant.[48]

Occasionally, PFM technique may present difficulties for the quantitative analysis of the piezoelectric coefficient d_{33}, mainly based on wrong electromechanical responses either of the AFM tip or of the electrostatic force from the system that do not depend exclusively on the piezo signal but on other physical effects. To overcome these problems, we compared our previous converse PFM analyses on BFO films with Direct Piezoelectric Force Microscopy (DPFM) measurements, which provides a direct and quantitative value of the piezoelectric constant in piezoelectric thin films.[37] The use of the DPFM method allowed us to collect, for the first time, the piezo-generated charge maps in a natural domain structure of a 60 nm thick epitaxial BFO film grown by the PAD process, see **Figure 5a** for DPFM-Si and DPFM-So. DPFM-Si stands for Signal Input, which is the current recorded while in trace mode and DPFM-So stands for Signal Output, collected while in retrace mode. In this measurement, the applied force exerted by the tip was varied along the scan, starting from the bottom of the frame, with forces (870, 174, 1218, 174, 1566 and 870 µN) see the dashed lines that delimiter each load that correspond to the upper part of the images.

Despite the big load, the large tip-sample contact area of this method notably reduces the pressure exerted by the tip. Therefore, the stress of the applied force stays below the plastic deformation limit of BFO.[37] The scan was performed at a speed of 31 µm/s with a resolution of 512x512 pixels ensuring that the transimpedance amplifier of the DPFM setup still acts as a current-to-voltage converter and not as a charge amplifier.[37] The specific pixel clock time, τ = 0.005s, was used to multiply the current scale and provide the scale bar in charge units. We were able to calculate the average maximum and minimum charge value recorded, as I * τ,[37] for each of the applied forces, see **Figure 5b**. Although the charge values obtained from this approximation cannot be used to quantify the d_{33} value accurately, as they do not integrate the full profile, they can be used to study the generated charge versus the applied load, which follows a linear fitting with slope values of m+ = 3.2E-4 ± 0.6 fC/µN and m- = -2.5E-4 ± 0.3 fC/µN. The graphs show two different values for the 174 and 870 µN
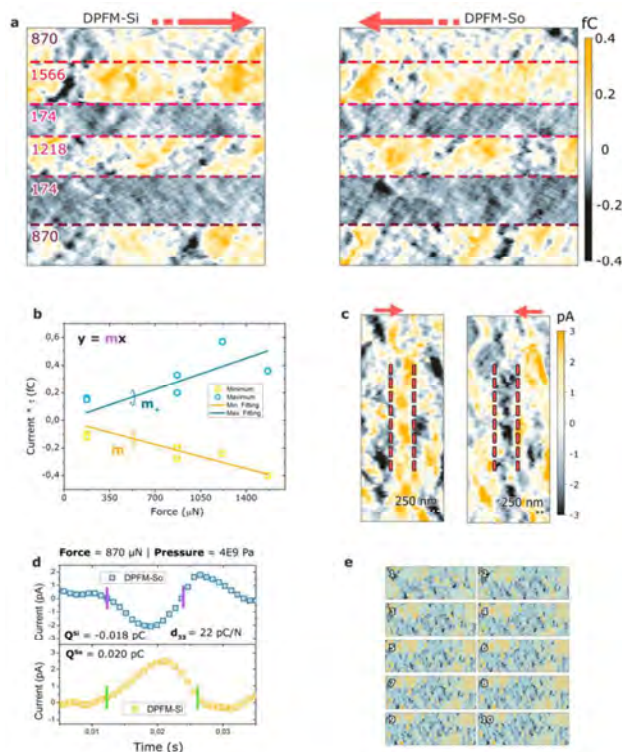

Figure 5. Piezogenerated charge mapping of a complex domain 60 nm thick BFO film. **a** DPFM-Si (left) and DPFM-So(right) obtained with different applying forces exerted by the probe. **b** corresponds to the representation of Current * τ vs Force obtained by acquiring the maximum value for each of the scanned areas in **5a**. **c**: Zoomed in region of DPFM-Si (left) and DPFM-So(right) obtained in an area of antiparallel domain configuration structure. The dashed lines mark the area that was used to obtain the average current profile depicted in **d.** The current profiles are integrated to find the piezogenerated charge of our films. **e** Collection of 10 consecutive frames applying a load of 870 µN, each frame taking approximately ~ 5 minutes.

values, as there are two different areas scanned at such load. Despite the highly localized measurements, it was possible to obtain a good approximation with a linear fitting, i.e. R^2 of 0.94 for the positive

slope and 0.85 for the negative one. This linear behavior is in agreement with the expected piezoelectric property of the sample.

Notice that the exact d_{33} measurement cannot be calculated from the linear fitting because the full current profile is not integrated. To overcome this limitation, we performed a zoom in a region over of the DPFM-Si and -So images that resembles crossing antiparallel domains, see **Figure 5c**. The average profiles from the areas denoted by the dashed lines were calculated using this approach. Two distinctive profiles were obtained, where the blue line corresponds to the averaged profile from DPFM-So image, the yellow line matches the averaged profile of DPFM-Si, see **Figure 5d**. In this figure, the current vs time is plotted in order to numerically integrate these profiles. The X axis, originally in metric units, is converted into time units by using the specific tip velocity, which is 31 µm/s. The numerical integration of such profiles gives the full collected charge, with -0.018pC and 0.020pC values for DPFM-So and -Si images, respectively. In order to

Journal Name

ARTICLE

calculate the d_{33} value in a direct way, we divided the average charge calculated for each DPFM-Si and DPFM-So images, referred to as Q^{SI} and Q^{SO}, by the applied force, which gave rise to a final d_{33} value of 22 pC/N. However, the large leakage current observed in our BFO thin films[49] (see **Figure S13**) prevents the measurement of the piezoelectric coefficient using macroscopic methods such as Double-Beam Laser Interferometry (DBLI). The obtained d_{33}^{DPFM} value is to our knowledge the first example of a direct quantitative measurement of the piezoelectric coefficient in BFO thin films. Importantly, d_{33}^{DPFM} value i.e. 22 pC/N is of the same order of magnitude as the d_{33} value previously obtained in bulk BFO material by using macroscopic methods i.e. from 16 to 60 pC/N.[8] Moreover, we observed an increased substrate clamping phenomenon in our BFO thin films compared to the 400 nm thick epitaxial BFO films[37] reducing the d_{33} value from 43 to 22 pC/N. Finally, we checked the reproducibility and the stability of the experiment by performing several scans in the same area at different times. Accordingly, 10 frame images were performed applying a load of 870 μN, each frame taking approximately ~ 5 minutes, see **Figure 5e**. Despite the high load applied, the data shows no degradation of the signal collected by the amplifier, confirming that the effective pressure exerted to the material does not surpass the plastic deformation limit or induce changes into the domain structure.[50, 51]

3. Experimental

Heteroepitaxial thin films of BFO ($a_{BFO}^{pc} = 3.965$ Å) were deposited on cubic (001) STO ($a_{STO} = 3.905$ Å) by PAD methodology from aqueous-based solutions. Individual solutions of Bi^{3+} and Fe^{3+} were prepared by dissolving their respective hydrated nitrates ($Bi(NO_3)_3.5H_2O$ and $Fe(NO_3)_3.9H_2O$) in deionized water with ethylenediaminetetraacetic acid (EDTA, 1:1 molar ratio) and polyethylenimine (PEI) (2:1 and 1:1 mass ratio to EDTA for Bi and Fe, respectively). The corresponding pH at room-temperature for these solutions was 8.1 for Bi and 5.1 for Fe. Each single solution was then filtrated three times using Amicon Ultrafiltration Cells (10 kDalton), and the retained portions were analyzed by Inductively Coupled Plasma Atomic Emission Spectroscopy (ICP-AES) yielding a final concentration of 79 and 200 mM for Bi and Fe, respectively. The filtrated solutions were mixed according to the final stoichiometry and concentrated to a final value of 0.25-0.3 M, in order to obtain films in the range 25-30-nm-thick range. It should be pointed out that cationic concentration is directly related to film thickness in PAD technique.[34] 30 μL of final solution with Bi/Fe (1:1) was spin coated (4000 rpm, 20 s) on 5 × 5 mm^2 (001) STO single-crystalline substrates. The samples were annealed in air/forming gas (H_2/N_2) at different temperatures (600°C-900°C) during 3 h with both slow heating and cooling ramps (1°C/min) to avoid the formation of cracks due to the plausible different coefficients of thermal expansion between STO ($9.0x10^{-6}K^{-1}$) and those reported for BFO (ranging from 6.5 to $13x10^{-6}K^{-1}$)[52, 53].

The thickness of BFO thin films was determined by X-Ray Reflectivity (XRR) in a *PANalytical Empyrean* diffractometer with an Euler cradle and using a Copper source with an incidence wavelength of 1.540598 Å. STEM and Electron Energy Loss Spectroscopy (EELS) analyses were carried out in a FEI Titan 60–300 microscope equipped with a high-brightness Schottky field emission gun (X-FEG), a CETCOR probe corrector from CEOS and a *Gatan* energy filter Tridiem 866 ERS operated in STEM at 300 kV. Specimens for STEM observation were prepared by grinding, dimpling, and Ar ion milling. The crystalline structure and the epitaxial relationship of the layers were studied by XRD in the same diffractometer, both in symmetric as in asymmetric configurations. Synchrotron XRD analysis at 20 keV and wavelength of 0.62 Å in a six-circle diffractometer were employed to further study the presence of impurities in the 600-650°C range. The surface quality of the films was verified by tapping Atomic Force Microscopy (AFM) images obtained using Park Systems NX-10 Scanning Probe Microscopy (SPM) unit.

The generation of the downward-oriented domains by electrical poling requires the existence of a conductive bottom electrode. The preparation of an epitaxial heterostructure containing a BFO top layer and a bottom electrode encompasses two steps, starting with the deposition of the conductive material. Typical materials employed as bottom conductive layers for BFO are $SrRuO_3$ (SRO) and $La_{0.7}Sr_{0.3}MnO_3$ (LSMO). We selected LSMO given its rhombohedral structure and similar lattice parameter ($a_{LSMO}^{pc} = 3.881$ Å) and we attempted the fabrication of both films by an entirely chemical solution route. The ≈20 nm-thick LSMO film was grown by PAD as described in[54] from a 0.2 M solution at 950°C. After the LSMO electrode is grown, the BFO layer was deposited and annealed as described previously increasing the thickness up to 60 nm to prevent leakages current.

PFM measurements were performed on an Agilent 5500LS instrument using a solid platinum conducting tip with a spring constant of 18 N m^{-1} and 80 μm tip length, (reference RMN-25PT300) with the aim of preventing artifacts not related to piezoelectricity.[55] The tip was biased with 4 VAC, while the DC bias was applied to the sample. The measurements were carried out away from the resonance frequency to avoid possible frequency-shifting artifacts. A Pt/Ir coated tip was employed to acquire the Amplitude vs Frequency plots presented in this work so the measurements are comparable with the ones presented in the current literature.

DPFM measurements were carried out in the same equipment as PFM. A special low leakage amplifier was used, based in *Analog Devices ADA4530*, with feedback resistor of 10 GOhm. A cascade voltage amplifier was used at the output of the transimpedance amplifier to increase the overall gain of the system. The amplifier provides enough bandwidth (159 Hz) to obtain the necessary data throughput for the images presented in this work. After the measurements, the amplifier was calibrated with a 100 GOhm resistor with part number MOX1125231009FE with 1% error. A suitable DC bias was applied through one side of the resistor and the inverting input of the amplifier, while the output signal from the cascade

ARTICLE   **Journal Name**

amplifier was recorded. To obtain the images, a *Rockymountain Nanotechnology* probe with part number RMN-25PtIr200H was used, while, to obtain the force, a common force-vs-distance curve was obtained to acquire the deflection sensitivity, and the force, multiply the sensitivity by the cantilever spring constant.

Conclusions

We have grown epitaxial BFO thin films by an aqueous-based solution route at 650°C with a crystalline quality comparable to those grown by physical methods, and with ferroelectric properties suitable for memory storage and piezoelectric devices. Besides, epitaxial BFO films grown by PAD present a higher natural domain size distribution and coercive field. The inversion of the BFO ferroelectric domains (180°) has been observed by PFM using LSMO bottom electrodes fabricated altogether by PAD. DPFM microscopy made possible to collect alternative measurements of the d_{33} constant of very thin film ferroelectric BFO samples with a direct approach. For the first time, piezo-generated charge maps of a very thin BFO layer with a complex domain structure were obtained by DPFM microscopy. The obtained d_{33}^{DPFM} value (22 pC/N) is in accordance with the converse d_{33}^{PFM} one (17 pm/V). Moreover, we have proved that the directionality of the piezoelectric effect in ferroelectric thin films is preserved at low thickness dimensions. This is an extraordinary advantage for the fabrication of nanometer-thick ferroelectric heterostructures using low-cost and versatile methodologies.

Conflicts of interest

There are no conflicts to declare.

Acknowledgements

References

1. G. H. Haertling, *J Am Ceram Soc*, 1999, **82**, 797-818.
2. J. M. Moreau, C. Michel, R. Gerson and W. J. James, *Journal of Physics and Chemistry of Solids*, 1971, **32**, 1315-1320.
3. D. Lebeugle, D. Colson, A. Forget and M. Viret, *Appl Phys Lett*, 2007, **91**.
4. F. Kubel and H. Schmid, *Acta Crystallographica Section B*, 1990, **46**, 698-702.
5. S. H. Baek and C. B. Eom, *Philosophical Transactions of the Royal Society A: Mathematical, Physical and Engineering Sciences*, 2012, **370**, 4872-4889.
6. J. Wang, J. B. Neaton, H. Zheng, V. Nagarajan, S. B. Ogale, B. Liu, D. Viehland, V. Vaithyanathan, D. G. Schlom, U. V. Waghmare, N. A. Spaldin, K. M. Rabe, M. Wuttig and R. Ramesh, *Science*, 2003, **299**, 1719-1722.
7. D. H. Kim, H. N. Lee, M. D. Biegalski and H. M. Christen, *Appl Phys Lett*, 2008, **92**.
8. G. Catalan and J. F. Scott, *Adv Mater*, 2009, **21**, 2463-2485.
9. X. Qi, J. Dho, R. Tomov, M. G. Blamire and J. L. MacManus-Driscoll, *Appl Phys Lett*, 2005, **86**, 062903.
10. C. Kittel, *Physical Review*, 1946, **70**, 965-971.
11. Y. B. Chen, M. B. Katz, X. Q. Pan, R. R. Das, D. M. Kim, S. H. Baek and C. B. Eom, *Appl Phys Lett*, 2007, **90**.
12. M. Valant, A. K. Axelsson and N. Alford, *Chem. Mater.*, 2007, **19**, 5431-5436.
13. J. X. Zhang, Q. He, M. Trassin, W. Luo, D. Yi, M. D. Rossell, P. Yu, L. You, C. H. Wang, C. Y. Kuo, J. T. Heron, Z. Hu, R. J. Zeches, H. J. Lin, A. Tanaka, C. T. Chen, L. H. Tjeng, Y. H. Chu and R. Ramesh, *Phys Rev Lett*, 2011, **107**.
14. A. Q. Jiang, C. Wang, K. J. Jin, X. B. Liu, J. F. Scott, C. S. Hwang, T. A. Tang, H. B. Lu and G. Z. Yang, *Adv Mater*, 2011, **23**, 1277-1281.
15. J. Li, J. Wang, M. Wuttig, R. Ramesh, N. Wang, B. Ruette, A. P. Pyatakov, A. K. Zvezdin and D. Viehland, *Appl Phys Lett*, 2004, **84**, 5261-5263.
16. C. Wang, K. J. Jin, Z. T. Xu, L. Wang, C. Ge, H. B. Lu, H. Z. Guo, M. He and G. Z. Yang, *Appl Phys Lett*, 2011, **98**.
17. R. R. Das, D. M. Kim, S. H. Baek, C. B. Eom, F. Zavaliche, S. Y. Yang, R. Ramesh, Y. B. Chen, X. Q. Pan, X. Ke, M. S. Rzchowski and S. K. Streiffer, *Appl Phys Lett*, 2006, **88**.
18. H. W. Jang, D. Ortiz, S. H. Baek, C. M. Folkman, R. R. Das, P. Shafer, Y. Chen, C. T. Nelson, X. Pan, R. Ramesh and C. B. Eom, *Adv Mater*, 2009, **21**, 817-823.
19. W. Ji, K. Yao and Y. C. Liang, *Adv Mater*, 2010, **22**, 1763-1766.
20. R. J. Zeches, M. D. Rossell, J. X. Zhang, A. J. Hatt, Q. He, C. H. Yang, A. Kumar, C. H. Wang, A. Melville, C. Adamo, G. Sheng, Y. H. Chu, J. F. Ihlefeld, R. Erni, C. Ederer, V. Gopalan, L. Q. Chen, D. G. Schldin, N. A. Spaldin, L. W. Martin and R. Ramesh, *Science*, 2009, **326**, 977-980.
21. J. F. Ihlefeld, N. J. Podraza, Z. K. Liu, R. C. Rai, X. Xu, T. Heeg, Y. B. Chen, J. Li, R. W. Collins, J. L. Musfeldt, X. Q.

Please do not adjust margins Nanoscale

Journal Name ARTICLE

Pan, J. Schubert, R. Ramesh and D. G. Schlom, *Appl Phys Lett*, 2008, **92**.

22. H. Béa, S. Fusil, K. Bouzehouane, M. Bibes, M. Sirena, G. Herranz, E. Jacquet, J. P. Contour and A. Barthélémy, *Japanese Journal of Applied Physics, Part 2: Letters*, 2006, **45**, L187-L189.

23. F. F. Lange, *Science*, 1996, **273**, 903-909.

24. S. K. Singh, Y. K. Kim, H. Funakubo and H. Ishiwara, *Appl Phys Lett*, 2006, **88**.

25. S. Iakovlev, C. H. Solterbeck, M. Kuhnke and M. Es-Souni, *J Appl Phys*, 2005, **97**.

26. Q. Zhang, N. Valanoor and O. Standard, *J Appl Phys*, 2014, **116**.

27. Q. Zhang, N. Valanoor and O. Standard, *Journal of Materials Chemistry C*, 2015, **3**, 582-595.

28. I. Bretos, R. Jiménez, D. Pérez-Mezcua, N. Salazar, J. Ricote and M. L. Calzada, *Adv Mater*, 2015, **27**, 2608-2613.

29. Q. Zhang, D. Sando and V. Nagarajan, *Journal of Materials Chemistry C*, 2016, **4**, 4092-4124.

30. Q. X. Jia, T. M. McCleskey, A. K. Burrell, Y. Lin, G. E. Collis, H. Wang, A. D. Q. Li and S. R. Foltyn, *Nat Mater*, 2004, **3**, 529-532.

31. J. M. Vila-Fungueiriño, B. Rivas-Murias, B. Rodríguez-González and F. Rivadulla, *Chem. Mater.*, 2014, **26**, 1480-1484.

32. J. M. Vila-Fungueiriño, B. Rivas-Murias, B. Rodríguez-González, O. Txoperena, D. Ciudad, L. E. Hueso, M. Lazzari and F. Rivadulla, *ACS Appl. Mater. Interfaces*, 2015, **7**, 5410-5414.

33. M. Jain, P. Shukla, Y. Li, M. F. Hundley, H. Wang, S. R. Foltyn, A. K. Burrell, T. M. McCleskey and Q. Jia, *Adv Mater*, 2006, **18**, 2695-2698.

34. J. Vila-Fungueirino, B. Rivas-Murias, J. Rubio-Zuazo, A. Carretero-Genevrier, M. Lazzari and F. Rivadulla, *Journal of Materials Chemistry C*, 2018, DOI: 10.1039/C8TC00626A.

35. H. Ɓa, M. Bibes, A. BartɦÍmy, K. Bouzehouane, E. Jacquet, A. Khodan, J. P. Contour, S. Fusil, F. Wyczisk, A. Forget, D. Lebeugle, D. Colson and M. Viret, *Appl Phys Lett*, 2005, **87**.

36. N. Pavlovic, J. D'Haen, H. Modarresi, A. Riskin, C. De Dobbelaere, M. J. Van Bael, K. Temst, A. Hardy and M. K. Van Bael, *J Mater Sci*, 2015, **50**, 4463-4476.

37. A. Gomez, M. Gich, A. Carretero-Genevrier, T. Puig and X. Obradors, *Nature Communications*, 2017, **8**.

38. D. A. Bonnell, S. V. Kalinin, A. L. Kholkin and A. Gruverman, *MRS Bull*, 2009, **34**, 648-657.

39. Y. Ahn, J. Seo, J. Yeog Son and J. Jang, *Materials Letters*, 2015, **154**, 25-28.

40. S. V. Kalinin, B. J. Rodriguez, S. Jesse, J. Shin, A. P. Baddorf, P. Gupta, H. Jain, D. B. Williams and A. Gruverman, *Microsc. Microanal.*, 2006, **12**, 206-220.

41. A. Lubk, S. Gemming and N. A. Spaldin, *Phys. Rev. B Condens. Matter Mater. Phys.*, 2009, **80**.

42. A. Bhatnagar, A. Roy Chaudhuri, Y. Heon Kim, D. Hesse and M. Alexe, *Nature Communications*, 2013, **4**.

43. N. Balke, P. Maksymovych, S. Jesse, A. Herklotz, A. Tselev, C. B. Eom, I. I. Kravchenko, P. Yu and S. V. Kalinin, *ACS Nano*, 2015, **9**, 6484-6492.

44. L. You, P. Caesario, L. Fang, P. Ren, L. Wang, Y. Zhou, A. Gruverman and J. Wang, *Phys. Rev. B Condens. Matter Mater. Phys.*, 2014, **90**.

45. J. L. Zhao, H. X. Lu, J. R. Sun and B. G. Shen, *Physica B: Condensed Matter*, 2012, **407**, 2258-2261.

46. A. Gruverman and S. V. Kalinin, *J Mater Sci*, 2006, **41**, 107-116.

47. S. V. Kalinin, A. Rar and S. Jesse, *IEEE Transactions on Ultrasonics, Ferroelectrics, and Frequency Control*, 2006, **53**, 2226-2251.

48. A. Gomez, H. T. Nong, S. Mercone, T. Puig and X. Obradors, *arXiv preprint arXiv:1711.11262*, 2017.

49. S. Gupta, M. Tomar, A. James and V. Gupta, *J Mater Sci*, 2014, **49**, 5355-5364.

50. A. Gómez, J. M. Vila-Fungueiriño, R. Moalla, G. Saint-Girons, J. Gázquez, M. Varela, R. Bachelet, M. Gich, F. Rivadulla and A. Carretero-Genevrier, *Small*, 2017, **13**.

51. H. Lu, C. W. Bark, D. Esque De Los Ojos, J. Alcala, C. B. Eom, G. Catalan and A. Gruverman, *Science*, 2012, **335**, 59-61.

52. J. D. A. U. R. B. K. Bucci and W. J. N. James, *Journal of Applied Crystallography*, **5IS - 3**, 187-191PY - 1972.

53. W. L. Wang and J. B. Li, *J Alloys Compd*, 2008, **459**, 70.

54. J. M. Vila-Fungueiriño, C. T. Bui, B. Rivas-Murias, E. Winkler, J. Milano, J. Santiso and F. Rivadulla, *J Phys D*, 2016, **49**.

55. S. V. Kalinin and D. A. Bonnell, *Phys. Rev. B Condens. Matter Mater. Phys.*, 2002, **65**, 1254081-12540811.

This journal is © The Royal Society of Chemistry 20xx
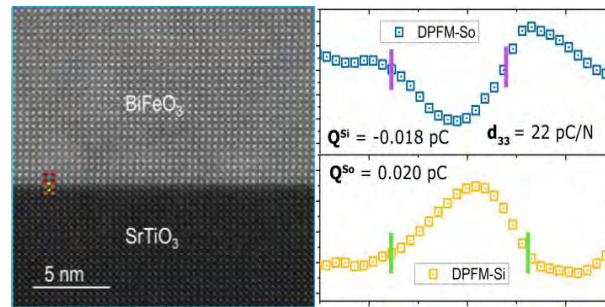
Nanoscaled direct and converse piezoelectric responses from sub-100 nm thick epitaxial $BiFeO_3$ thin films grown by a water-based chemical method